ADVANCED QUANTUM TECHNOLOGIES
www.advquantumtech.com

A Temperature Study of High-*n* Rydberg States in Cu_2O

*Julian Heckötter, Binodbihari Panda, Katharina Brägelmann, Marc Aßmann, and Manfred Bayer**

The temperature dependence of Rydberg excitons in Cu_2O with principal quantum numbers $n \geq 10$ is investigated for bath temperatures between 1.3 and 50 K. The energy shift of Rydberg exciton lines allows us to perform a precise measurement of the Cu_2O band gap as a function of temperature. The Γ_5^- phonon shows a dominant contribution to the temperature shift of the band gap. The optical properties of Rydberg excitons are analyzed for different temperatures and discussed in the context of phonon scattering as well as thermal ionization of impurities and compared to earlier descriptions in Ref. [1]. The maximum principal quantum number n_{max} as a function of temperature in crystals of different quality is studied and compared. The observations are correlated to photoluminescence spectra of impurities at different temperatures.

1. Introduction

Atoms with at least one electron in an highly-excited state are called Rydberg atoms. They exhibit exceptional physical properties that serve as the basis for a variety of concepts in quantum optics[2,3] and quantum information processing.[4] In an excited state with high principal quantum number n, their dipole moments exceed those of ground state atoms by orders of magnitudes, resulting in strong long-range interactions among different Rydberg states.[5] Moreover, Rydberg atoms are highly sensitive to external electric and magnetic fields which renders them highly efficient sensors.[6]

Rydberg excitons are the solid-state analogue to Rydberg atoms. They consist of electron hole pairs in semiconductors excited to high principal quantum numbers n and are promising candidates for studying Rydberg physics in the solid state.[7] Rydberg excitons with high principal quantum numbers, such as $n =$ 25 to 30, can be observed in the semiconductor Cu_2O.[8,9] During the past years, researchers observed strong interactions[10,11] and huge optical nonlinearities[12] for Rydberg excitons in this material. Their polarizability grows as n^7,[13] which renders these states sensitive to external charges. Krüger et al.[14] showed that even smallest densities of charged impurities on the order of 0.001 μm^{-3} introduce inhomogeneous electric microfields that are sufficient to disturb high-n states and reduce the number of observable lines. Also, plasmas consisting of electron-hole pairs with densities of the same order of magnitude are sufficient to destroy the highest n.[15]

Since most of the Rydberg excitons' unique properties scale characteristically with n,[13] being able to excite states with principal quantum numbers as high as possible is of fundamental interest. So far, Rydberg excitons with principal quantum numbers $n > 20$ have been observed solely in naturally grown crystals. Experiments are typically performed at liquid helium temperatures of ≈1.3 K. At higher temperatures the maximum observable principal quantum number decreases.[1,16] In order to achieve higher principal quantum numbers, experiments were also performed at millikelvin temperatures where excitons with $n = 28$[17] and $n = 30$[9] have been observed. These experiments showed that at these low temperatures the limit of observable states is rather given by the crystal quality than by thermal dissociation.[17]

However, many of the technologically relevant properties of Rydberg excitons can already be exploited at intermediate n, and so Kang et al.[16] recently investigated the high-temperature behavior up to 100 K for states with principal quantum number $n = 5$ to 11. The observation of higher states was limited by the resolution of their spectrometer.

In ref. [1] we studied the highest observable principal quantum number, n_{max}, for different bath temperatures reaching from 1.3 to 50 K, measured with a narrow bandwidth laser. In that study, thermal dissociation by acoustical phonons was considered as the limiting dissociation process explaining the data quite well. However, Stolz et al.[18] showed that thermal dissociation by acoustical phonons is expected to be negligible for states with n smaller than $n = 30$. Even at 20 K it is supposed to be relevant for $n > 24$ only. Hence, the question remains why Rydberg excitons vanish with temperature. Besides thermal dissociation, also ionized impurities[14] as well as an electron-hole plasma[19] are considered as limiting factors for the highest observable quantum number.

Here, we discuss the change of the Rydberg exciton absorption spectrum with increasing temperature for states with $n \geq 10$. We revisit the data from ref. [1] and provide a thorough

J. Heckötter, B. Panda, K. Brägelmann, M. Aßmann, M. Bayer
TU Dortmund University
14311, Otto-Hahn Strasse 4a, 44227 Dortmund, NRW, Germany
E-mail: manfred.bayer@tu-dortmund.de

The ORCID identification number(s) for the author(s) of this article can be found under https://doi.org/10.1002/qute.202300426

DOI: 10.1002/qute.202300426

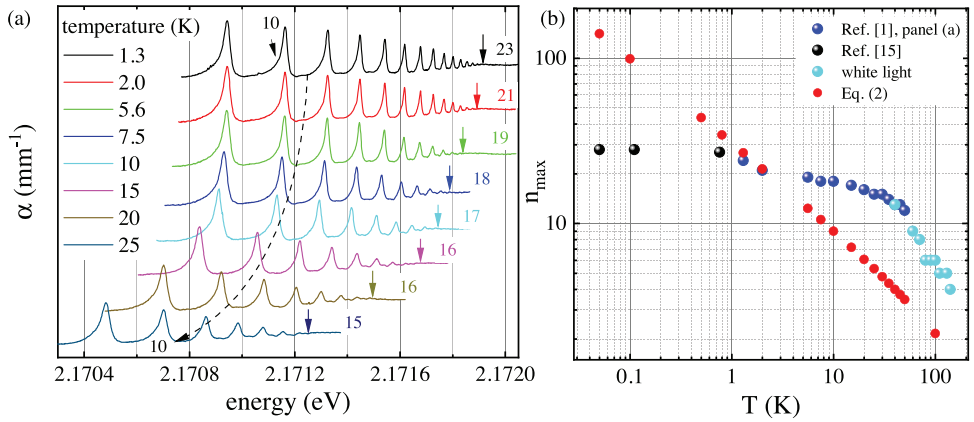

Figure 1. a) Rydberg exciton states from $n = 9$ to the band gap for different temperatures in the high-quality sample I. The spectra are vertically shifted for clarity. With increasing temperature the spectra shift to lower energies and the highest observable quantum number n_{max} changes. Vertical arrows indicate the apparent band gap $\tilde{E}_g$. Figure adapted from ref. [1]. b) Principal quantum number n_{max} of the highest observable Rydberg exciton state as a function of temperature in a high-quality sample (black and blue dots) compared to the estimated value via $k_B T = Ryd/n^2$ (red dots).

analysis of parameters such as energy shift, linewidths and oscillator strengths. We show that the interaction between Γ_5^- phonons and Rydberg excitons is decisive for the exciton spectrum at elevated temperatures, but also charged impurities play a dominant role below 30 K. We reinterpret the thermally induced band gap shift and compare it for samples of different quality. We find that the total shift of the continuum edge is stronger than the bare thermal shift of exciton lines and identify correlations between the difference and the thermal activation of impurities. We complement the data by measurements of impurity-related photoluminescence.

2. Experimental Section

2.1. Experimental Setup

The transmission of thin Cu_2O slabs was measured by tuning the wavelength of a narrow-bandwidth dye laser. Throughout this study, three different samples were used. They differ in quality, which translates to the number of observable exciton lines in the Rydberg exciton absorption spectrum. Sample I was a high-quality natural crystal from Namibia with a thickness of 30 µm, used for example in refs. [8, 17]. Sample II was of lower quality and artificially grown.[20,21] It has a thickness of 50 µm and shows prominent impurity-related features (see also ref. [22]). Sample III was a natural sample with a thickness of 30 µm, but of lower quality compared to sample I.

The laser beam was focused onto the samples with a spot diameter of 100 µm and a power of 1 µW. The transmitted light was collimated and detected by a photodiode. The samples were placed in a cryostat and surrounded by liquid helium. Additional pumping may lower the bath temperature to 1.3 K. Higher temperatures were achieved by automated control of helium flow and heating.

Photoluminescence was detected by a Acton SpectraPro-500i spectrometer with a resolution of 0.5 meV covering the spectral range from 850–600 nm.

3. Results and Discussion

3.1. Maximal Observable Quantum Number n_{max}

Figure 1a shows the temperature dependence of *P*-envelope Rydberg exciton states from $n = 9$ to the band gap for various temperatures from 1.3 to 25 K for the high-quality sample I. The figure is adapted from ref. [1]. At the lowest temperature of 1.3 K, absorption lines of Rydberg excitons up to principal quantum number $n = 23$ can be observed, as shown by the black curve. The lines form a Rydberg series below the band gap E_g with resonance energies following to a good approximation.

$$E_X(n) = E_g(T) - Ryd/n^2 \quad (1)$$

Here, $Ryd = 90$ meV is the Rydberg energy and Ryd/n^2 is the binding energy of a state with principal quantum number n. For 1.3 K one finds $E_g = 2.17208$ eV[8] by fitting the Rydberg exciton series according to Equation (1). With increasing n, both the oscillator strengths and the linewidths decrease as n^{-3} according to literature.[8] The highest exciton lines typically loose oscillator strength stronger than predicted by this scaling and show an inhomogeneous broadening. Thus, while approaching the band gap, the absorption per exciton line decreases and eventually the absorption turns into a flat continuum. The energy at which the Rydberg exciton series ends is typically referred to as the apparent band gap $\tilde{E}_g$. Its value is lower than the nominal band gap E_g. Apparently, $\tilde{E}_g$ is not constant and closely related to the highest observable quantum number n_{max}. It is heavily influenced by the crystal quality in terms of strain and the density of impurities[14] (see Equation (9) below). At 1.3 K, we find $\tilde{E}_g = 2.17193$ eV.

With increasing temperature, all Rydberg exciton lines shift towards lower energies. At 25 K, this shift amounts to ≈460 µeV, as indicated by the dashed arrow in panel (a). In a similar way, the continuum edge $\tilde{E}_g$ is redshifted as well and n_{max} decreases. For all temperatures, $\tilde{E}_g$ is indicated by individual arrows. Before we analyze the energy shifts quantitatively, we present the observed n_{max} as a function of temperature in Figure 1b. The values

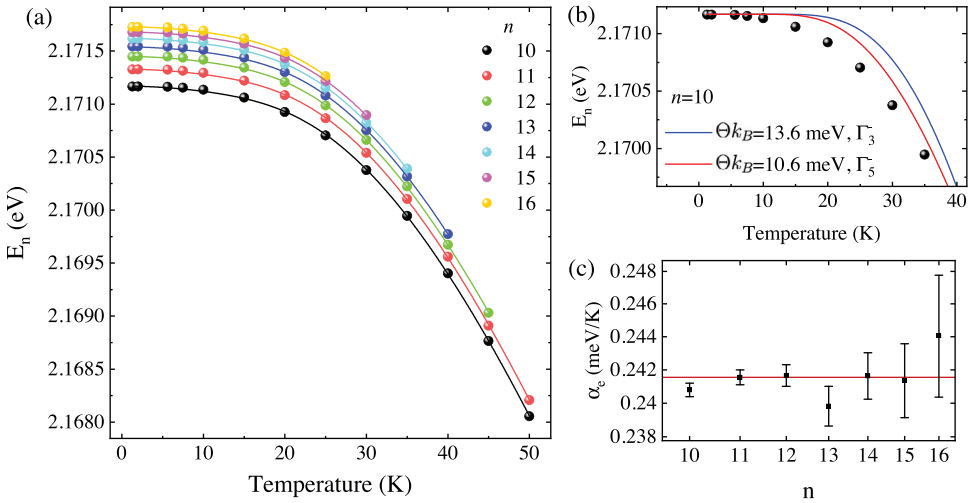

Figure 2. a) Energy shift of nP states (dots) and fits (lines) according to Equation (5). b) An example of fit according to Equation 4 using phonon energies of the two lowest optical phonons. The formula fails to reproduce the data at temperatures below 40 K. c) Variation of coefficient α of the fit in panel a) and mean value indicated by the red line.

obtained from panel (a) are shown as blue dots. The data is complemented with values measured at millikelvin temperatures, as discussed in ref. [17], drawn as black dots. From 50 to 140 K, the data is extended by values measured using a broadband white light source and a double spectrometer with 10 µeV resolution (bright blue dots). At 140 K, we find $n_{max} = 4$. The data is compared to the limit expected when assuming that thermal dissociation becomes efficient, i.e. when the thermal energy $k_B T$ matches the Rydberg energy Ryd/n^2:

$$n_{\mathrm{max,th}} \approx \sqrt{\frac{Ryd}{k_B T}} \tag{2}$$

that is shown by the red dots. For temperatures below 1 K, the maximum observable n is lower than the thermal limit given by Equation (2), suggesting that other limiting effects, such as impurities and crystal quality also play a role. Between 1 and 2 K the highest quantum number observed in experiment agrees quite well with the estimate given by Equation (2). Noteworthy, at temperatures above 2 K the maximal observed quantum number is actually higher than given by the simple estimate via $k_B T$.

3.2. Temperature Shift of the Band Gap

Now, we discuss the redshift of exciton lines more quantitatively. The data in Figure 1 is analyzed by fitting asymmetric lorentzians to the data according to[23,24]

$$\alpha_n = C_n \frac{\Gamma_n/2 + 2q_n(E - E_n)}{(\Gamma_n/2)^2 + (E - E_n)^2} \tag{3}$$

where Γ_n is the linewidth, C_n is the oscillator strength and q_n is an asymmetry parameter of an exciton with principal quantum number n. E_n is the resonance energy. **Figure** 2a shows the obtained resonance energies of the nP states from $n = 10$ to 16 as a function of temperature. From 1.3 to 50 K, the exciton lines shift in total by ≈3.12 meV to lower energies. Assuming a constant Rydberg energy Ryd, this shift reflects the temperature dependence of the nominal band gap $E_g(T)$, see Equation (1).

Based on a Bose-Einstein phonon model, the temperature shift of the band gap can be described by the following dependence[25]

$$E_g(T) = E_{g0} - \alpha_e \Theta \left(\coth\left(\frac{\Theta}{2T}\right) - 1 \right) \tag{4}$$

with the temperature-independent band gap E_{g0}, the coupling constant α_e and the energy of the involved phonon $k_B\Theta$.[26] Sun et al.[27] and Kang et al.[16] successfully used this approach in their studies to describe the temperature shifts of the yellow 1S exciton and the yellow and green band gaps up to 100 K with a phonon energy of $\Theta k_B = 13.6$ meV for the strong Γ_3^- optical phonon in Cu_2O. Figure 2b shows a fit to our data according to Equation 4 with $\hbar\omega = 13.6$ and 10.6 meV, i.e. the energy of the Γ_3^- and Γ_5^- optical phonons with lowest energy in Cu_2O. Interestingly, we find a solid mismatch between the fits and data. The experimentally observed shift is stronger than the one described by the fits.

A more sophisticated model for the temperature shift of the band gap was given in ref. [28], which takes variable phonon-dispersions into account, comprised in a dispersion coefficient Δ.[26] Here, the shift is described by

$$E_g(T) = E_{g0} - \alpha_e \bar{\Theta} \left[\frac{1 - 3\Delta^2}{\exp(2/\gamma) - 1} + \frac{3\Delta^2}{2} \left(\sqrt[6]{1 + \beta} - 1 \right) \right] \tag{5}$$

$\bar{\Theta}$ is an average phonon energy and used as a fit parameter here. $\beta = \frac{\pi^2}{3(1+\Delta^2)}\gamma^2 + \frac{3\Delta^2-1}{4}\gamma^3 + \frac{8}{3}\gamma^4 + \gamma^6$ and $\gamma = 2T/\bar{\Theta}$. Using this approach, we can describe the energy shifts of the Rydberg exciton lines in Figure 2a quite well, as shown by the solid lines. The fit parameters are listed in **Table** 1. Among all n, the coefficient α_e varies within 2% around the average value $\bar{\alpha}_e$, see Figure 2c. The fit reveals $\bar{\Theta} \approx 123$ K, which translates to a phonon energy

Table 1. Parameters for the temperature dependence of the band gap E_g in Cu_2O obtained by a fit to the Rydberg exciton energies of the states from $n = 10$ to $n = 16$ according to Equation (5).

$\bar{\alpha}_\varepsilon$ (10^{-4}eV/K)	Θ (K)	Θk_B (meV)	Δ
2.41558	123.10567	10.59	0.29352

of $\bar{\Theta}k_B \approx 10.6$ meV. This energy agrees very well with the energy of the Γ_5^- optical phonon in Cu_2O. Inclusion of other phonons, such as the Γ_3^- phonon with an energy of 13.6 meV, leads to a larger deviation between data and model. In the following we write Θ instead of $\bar{\Theta}$. Moreover, we find for the dispersion coefficient $\Delta \approx 0.29$.

We note that also other models have been proposed to describe the temperature dependence of the band gap: Varshni's formula[29] turns out to be rather inaccurate here as it differs from the data at low temperatures by ≈3 meV. Another model proposed in ref. [30] uses an optical and an acoustical phonon branch with fixed phonon energies. According to the phonon density of states of Cu_2O[31] the acoustic phonon branch at low energies is rather broad which renders the identification of a single mode cumbersome. The model described by Equation (5) is favored here, as the parameter Δ takes the width of a phonon branch into account.

3.3. Linewidths and Oscillator Strengths

Besides the resonance energies, also the linewidths and oscillator strengths change with temperature. In **Figure 3** we show the linewidths and oscillator strengths, obtained by a fit according to Equation (3), for states from $n = 10$ to 19 as a function of temperature. The data is vertically stacked for clarity. Stolz et al.[18] found that the linewidth should be temperature independent up to 50 K since the optical phonon energies are all above 10 meV and acoustical phonons contribute less than 1 % to the linewidth. However, the measured linewidths broaden strongly with increasing temperature even below 50 K in a non-trivial way, as described further below. As an example, the linewidth of the exciton with $n = 12$ grows by a factor more than 3 from 17 μeV at 1.3 K to 63 μeV at 40 K.

Typically, the temperature dependence of exciton linewidths can be expressed by[32]

$$\Gamma_n(T) = \Gamma_0 + \gamma_{ac} T + \Gamma_{op}/2\left[\coth\left(\Theta_i/2T\right) - 1\right] \quad (6)$$

where Γ_0 is determined by radiative and inhomogeneous widths. The second term describes scattering with acoustic phonons which increases linearly with temperature.[33] Following ref. [24], the last term describes the broadening induced by optical phonons, in analogy to the change of the band gap energy Equation (4). The last term was used by Kang et al. in ref. [16]. The authors were able to describe the linewidth broadening up to 100 K quite well using $\Theta k_B = 13.6$ meV.

Here, we use the extended model from Equation (5) to express the linewidth broadening by optical phonons. Moreover, we neglect scattering by acoustical phonons, as discussed further below, and end up with

$$\Gamma_n(T) = \Gamma_0 + \Gamma_{op}\Theta\left[\frac{1-3\Delta^2}{\exp(2/\gamma)-1} + \frac{3\Delta^2}{2}\left(\sqrt[6]{1+\beta}-1\right)\right] \quad (7)$$

We fit the data according to Equation (7) and fix Γ_0 for each n at 1.3 K. We use $\Theta = 123$ K (Γ_5^- phonon) and $\Delta = 0.294$, as obtained in Section 3.2, and keep Γ_{op} free. The resulting fits are shown as solid lines in Figure 3a, whereas we restrict the analysis to states with $n = 10$ to 15. Γ_{op} varies only slightly with n for states with $n = 10$ to 15, as shown in Figure 3b. The mean value we find is $\Gamma_{op} = 6.1$ μeV/K, as shown by the horizontal red line.

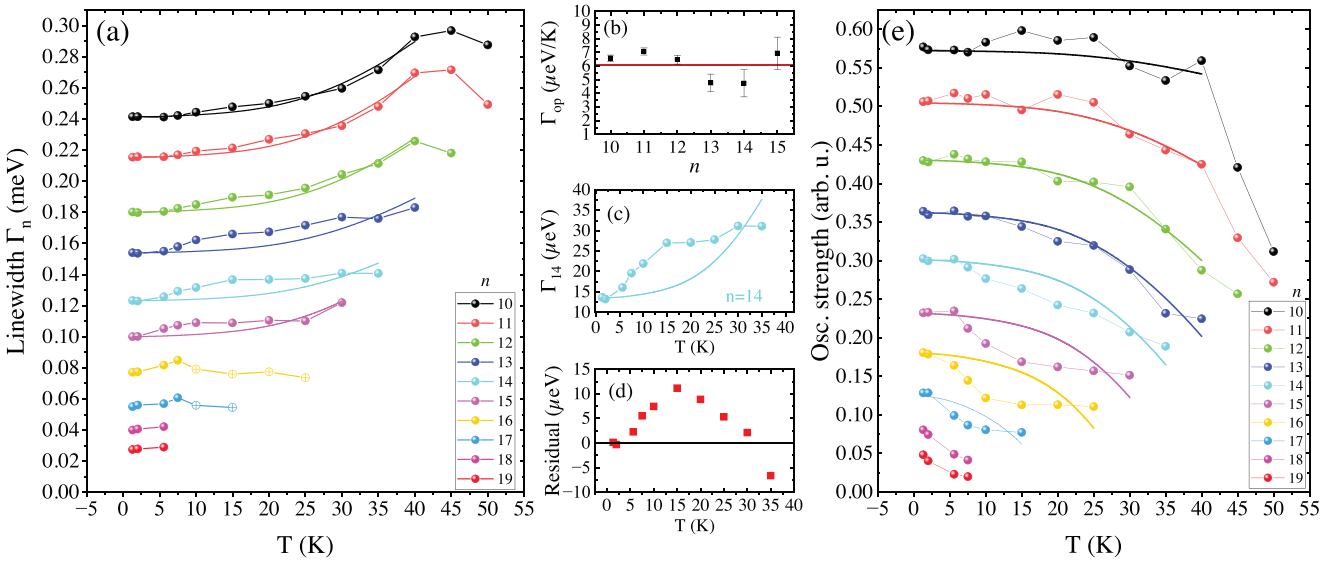

Figure 3. a) Linewidths (dots) as a function of temperature and fits (lines) according to Equation (7). The data is vertically shifted for clarity. Between 5 and 30 K the experimental linewidths deviate from the fits. b) Γ_{op} varies slightly among all fitted curves. The red line shows the mean value. c) Zoom into linewidths broadening of state $n = 14$. d) Residuals of the fitting procedure in panel (c). The fit deviates up to 30 μeV from the data. e) Same as (a) but for oscillator strengths. For all n, the oscillator strengths drop with temperature. The drop is stronger than described by the model for $n \geq 14$.

We find that Equation (7) reproduces the general trend of an increased linewidth broadening for the lower-n states with $n = 10$ and 11 well. However, for the higher states with $n = 12$ to 15, the model fails to describe the data between 5 and 30 K. For these states the experimentally observed broadening is stronger than given by pure phonon broadening. Up to 10 K, the linewidth increases linearly, whereas the slope becomes stronger for higher n. Between 15 and roughly 25 K the linewidths tend to flatten, which leads to a step-like dependence, before they further increase again from 25 K on. This can be seen in detail in Figure 3c for $n = 14$. The deviations from the fit result are shown in panel d. At 15 K the data deviates by about 10 μeV from the fit.

The linear increase at low temperatures could in principle also stem from acoustical phonons. We neglect it due to the following 2 reasons: As stated above, ref. [18] claims a negligible contribution of acoustical phonons to the linewidth. Moreover, the observed broadening saturates at 10 K (see panel (c)), which is not in line with a constant increase in T.

For completeness we note that at temperatures above 40 K, even a decrease of linewidths for the states $n = 10$–12 is observed. For states $n = 16$ and 17, we also find some anomalous behavior: After a strong increase of the linewidth up to ≈7.5 K the linewidths become narrower again. The states with $n = 18$ and 19 are also shown for completeness.

Kang et al.,[16] analyzed the temperature dependence of the oscillator strength as well. The authors did not find a significant change of the oscillator strength with temperature for the states from $n = 2$ to $n = 6$ up to a temperature of 100 K. In particular, they even found a small increase of the oscillator strength for the states $n = 2$, 5 and 6. We show the oscillator strength as a function of temperature for states $n = 10$ to 19 in Figure 3e. We observe a continuous drop of oscillator strength with temperature for these states. Following Kang et al., we try to describe the drop of oscillator strength in analogy to the linewidth broadening with an expression

$$C_n(T) = C_0 + C_{op}\Theta\left[\frac{1-3\Delta^2}{\exp(2/\gamma)-1} + \frac{3\Delta^2}{2}\left(\sqrt[6]{1+\beta}-1\right)\right] \quad (8)$$

We fit the data by Equation (8) and show the fits by the solid lines. For each n, C_0 is determined at $T = 1.3$ K. Again, we set $\Theta = 123$ K (Γ_5^- phonon) and $\Delta = 0.293$. While the fits describe the data reasonably well for states with low n, such as 10 to 13, they fail to reproduce the strong drop observed in the experiment for high-n states. In particular, the oscillator strength of states with $n = 14$ to 17 drops strongly between 1.3 K and 10 K and deviates from the phonon-model up to ≈30 K. Hence, phonon scattering as described by Equation (8) might not fully cover the complex physics of high-n Rydberg states at increasing temperatures. Here, a better model for the dependence of oscillator strength on temperature - including phonon scattering - might be necessary to describe the observations.

Concluding, the drop of oscillator strength as well as the broadening of linewidths with temperature are stronger than given by pure phonon-scattering which may imply another physical mechanism that affects the Rydberg exciton lines up to 30 K. Since the oscillator strengths and linewidths of highest Rydberg excitons depend strongly on the density of charged impurities in the sample,[14] a growing density of charged impurities caused by the increasing temperature seems to be a reasonable candidate.

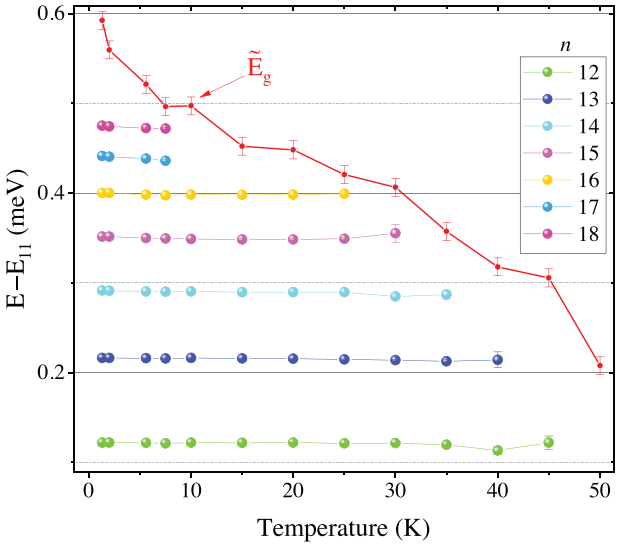

Figure 4. Difference in energy between the apparent band gap $\tilde{E}_g$ as well as exciton lines of certain quantum number n and the exciton with quantum number $n = 11$. Up to 45 K, the spectral separation of exciton lines does not change within 5 μeV accuracy. The apparent band gap $\tilde{E}_g$ shifts by about 400 μeV more than the exciton line with $n = 11$.

3.4. Impurity Density

In Section 3.1 we discussed the temperature dependence of the maximum observable principal quantum number n_{max}. Apparently, this value is closely connected to the energy of the apparent band gap $\tilde{E}_g$, i.e. the energy at which the absorption spectrum becomes flat and the continuum starts. This energy can be estimated from the absorption spectrum and is indicated by arrows in Figure 1a. In a naive picture one could assume that the shift of this energy with temperature might be comparable to the shift of the nP exciton lines or the nominal band gap E_g. Interestingly, we observe a much stronger shift of the apparent band gap relative to the shift of the exciton lines. To illustrate that deviation, we show the difference between $\tilde{E}_g$ and the energy of the $n = 11$ exciton at each temperature by the red line in **Figure 4**. Additionally, the differences between the energies of higher n and the $n = 11$ exciton are shown as well. The energy difference between the lines stays constant within 5 μeV up to a temperature of 40 K. We conclude that within this temperature range the Rydberg energy Ryd and with it the effective masses of electrons and holes as well as the dielectric constant hardly change. This is in agreement with the small variation in the coupling constant α_e over all n (see Section 3.2).

On the contrary, the apparent band gap shifts $\tilde{E}_g$ by ≈400 μeV more than the nP states between 1.3 and 50 K. In principle, a phonon-induced linewidth broadening can lead to an overlapping of high-n exciton lines which may merge into an apparent continuum. This may become relevant from 30 K onwards, where the linewidth broadening agrees with the phonon-scattering model. Below 30 K, however, we assume that

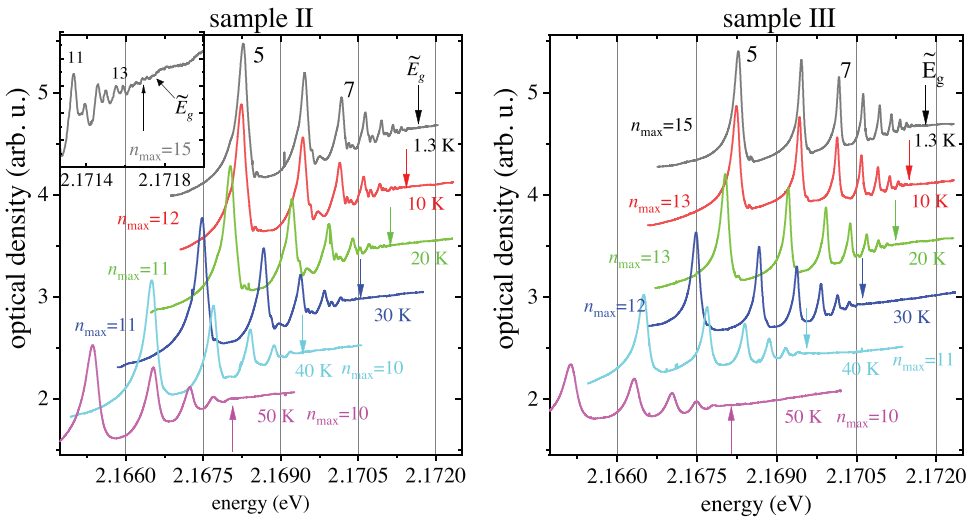

Figure 5. Temperature dependence of absorption spectra from $n = 5$ to the band gap for low-quality samples II a) and III b). The spectra are vertically shifted for clarity. The arrows mark the apparent band gap $\tilde{E}_g$ above which the Rydberg spectrum ends. The inset in panel a) shows a zoom into the high energy range of the spectrum at 1.3 K, where $n_{max} = 15$ can be observed.

the continuum energy $\tilde{E}_g$ and the highest principal quantum number n_{max} are dominated by another physical mechanism. A shift of the apparent band gap was reported in ref. [15] as a consequence of an increasing density of free carriers leading to a Mott-effect for high-n exciton lines. Moreover, a the apparent gap was shown to shift also with an increasing number of charged impurities in ref. [14] Based on the considerations in the previous chapter Section 3.3, we consider a temperature dependent activation of impurities to play a role here.

Before we compare the observed shift of $\tilde{E}_g$ with predictions by impurity-related models, we introduce two other samples II and III. These samples are of inferior quality compared to the previous one (see Section 2.1), which may result from a larger density of impurities. The resulting spectra are shown in **Figure 5** for sample II in panel (a) and sample III in panel (b). The lower quality of these samples manifests itself in the maximum principal quantum number that can be observed at a temperature of 1.3 K. For both samples $n_{max} = 15$. Qualitatively, the spectra and their change with temperature look similar. Sample II, however, shows prominent peaks in between the P exciton states, which we interpret as even angular momentum excitons that become optically allowed due to the presence of inhomogeneous electric fields induced by charged impurities.[22] All exciton lines shift to lower energies with increasing temperature. The apparent band gap and n_{max} are reduced as well, as indicated by the vertical arrows. Already at 10 K, n_{max} is as low as 12 (sample II) or 13 (sample III), while we were still able to observe $n_{max} = 18$ for the high-quality sample as shown in Figure 1.

At a temperature where phonon-related mechanisms become dominant and overcome the impact of impurities, n_{max} may become equal among the different samples. Therefore, we compare n_{max} and the change of $\tilde{E}_g$ for the three different samples in **Figure 6**a and b. Indeed, the difference in n_{max} among the samples becomes smaller with increasing temperature. At 50 K, n_{max} equals 10 for the low-quality samples II and III, while the high-quality sample I shows still 2 more lines. This is in line

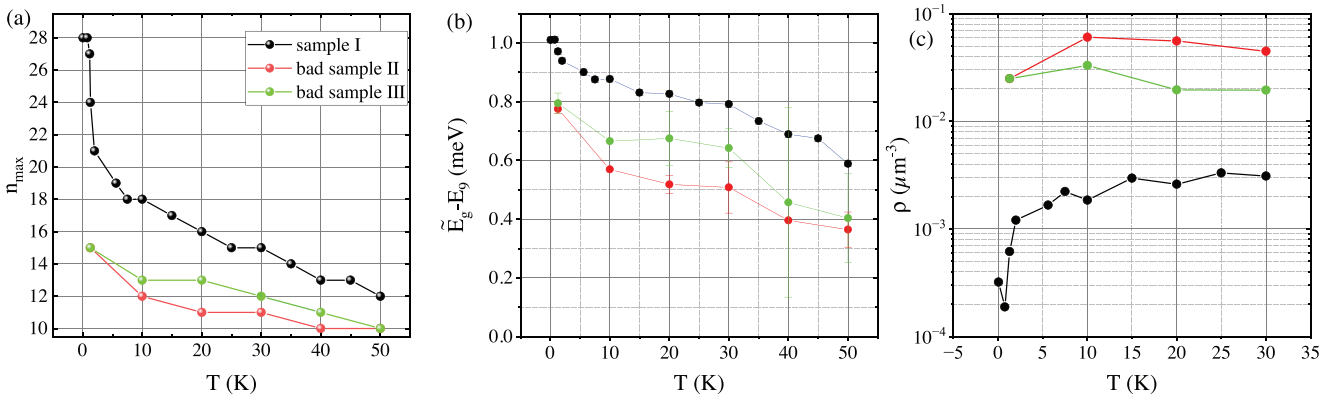

Figure 6. Comparison of samples I, II and III. a) n_{max} vs. temperature. b) Shift of the apparent band gap $\tilde{E}_g$ vs temperature. c) Density of impurities vs temperature. Calculated with Equations (9) and (10), assuming $\tilde{E}_g$ is mainly determined by the density of impurities and a single particle plasma up to 30 K.

with ref. [18], which expects optical phonon scattering to give relevant contributions to the linewidth broadening from temperatures ≈50 K on.

$\tilde{E}_g$ shows a shift in energy that is stronger than that of the $9P$ states in all three samples. As stated above, the stronger shift $\tilde{E}_g$ compared to the $9P$ state suggests that $\tilde{E}_g$ is affected strongly by an increasing density of charged impurities along with the creation of free carriers due to thermal ionization. Assuming a negligible impact of phonons up to 30 K, we can estimate the density of charged impurities from the measured band gap shifts in panel (b) as a function of bath temperature. Ref. [14] provides an analytic expression for the band gap shift as a function of density of charged impurities ρ_{ci}

$$\Delta E_g(\rho_{ci}) = -710\mu eV(\rho_{ci}/\mu m^{-3})^{1/4} \tag{9}$$

which is close to the band gap shift caused by a single particle plasma of density ρ_p, as given by Semkat et al.:[34]

$$\Delta E_g(\rho_p) = \frac{1}{\sqrt{2}} 692\mu eV \left(\rho_p/\mu m^{-3}\right)^{1/4} \left(T_p/K\right)^{1/4} \tag{10}$$

Here, T_p is the plasma temperature. The factor $1/\sqrt{2}$ arises from the fact that only a single-particle plasma is considered.[35] In the following we assume that the plasma is in thermal equilibrium with its environment and use $T_\rho = T$. If neutral impurities become ionized by thermal energy, residual charges may be released into the crystal. These charges then act like a low-density plasma and affect the apparent band gap $\tilde{E}_g$ in addition to the now also charged impurities themselves, according to Equation (11). Note, that taking such a residual plasma into account leads to lower values for impurity densities compared to previous estimations in ref. [14, 15].

The resulting densities of charged impurities are shown in Figure 6c up to 30 K in a semi-logarithmic representation for all three samples. The obtained density of impurities in sample I starts at around $2 \cdot 10^{-4} \mu m^{-3}$ at the lowest temperature of 760 mK and increases strongly up to $2 \cdot 10^{-3}$ μm^{-3} at 10 K. It tends to saturate around $3 \cdot 10^{-3}$ μm^{-3} at 30 K. To some extent, this trend is similar to the temperature dependence of the linewidths and oscillator strengths in Figure 3, where deviations between the experimental values and fits according to the phonon-model appeared up to 30 K. In particular, the linewidths show a similar steep increase up to 10 K and the oscillator strengths show a corresponding drop. Presumably, the saturation indicates a situation where most of the impurities with a low binding energy are thermally ionized and the corresponding density cannot increase further.

In samples II and III, the impurity density is around 2 orders of magnitude higher compared to sample I at 1.3 K. The density grows up to 10 K, followed by a small decrease at 20 and 30 K. This decrease is a consequence of the temperature dependence of the plasma-induced band gap shift in Equation (11), which becomes relevant as the measured band gap $\tilde{E}_g$ in panel b) stays almost constant within this temperature range.

3.5. Temperature Dependence of Impurity Photoluminescence

Up to this point we discussed the change of Rydberg exciton absorption spectra as a function of temperature. Next, we extend these investigations by a study of photoluminescence spectra of impurities for various temperatures, measured on the high-quality sample I. **Figure** 7a shows the photoluminescence between 1.4 and 2.03 eV for varying temperature from 1.3 to ≈60 K. The spectra are vertically shifted for clarity. The spectra consist of emission from singly- and doubly charged oxygen vacancies, centered around 1.5 and 1.7 eV, as well as the emission of the $1S$ ortho exciton at 2.03 eV and its phonon replica. An emission from copper vacancies is not observed, which is in agreement with other observations for natural crystals.[36,37] At 5 K, a broad emission band is observed between the phonon and the O^{++} line (indicated by the circle in panel (a)). According to refs. [36, 38, 39], the origin of this broad band are excitons bound to metallic impurities. We label this region as region C. Note that any features related to an emission associated with up-conversion from 1S para and ortho excitons[33] cannot be resolved here.

With increasing temperature, the prominent emission features from the oxygen vacancies grow until they saturate at ≈60 K. An increase of the oxygen vacancy emission is also seen in ref. [36] up to ≈70 K, albeit less pronounced. Another (tiny) increase between 20 and 40 K can be seen in ref. [40]. Compared to these studies, the increase observed in Figure 7a appears quite strong. The integrated intensities of oxygen vacancies are plotted in Figure 7c.

On the other hand, Koirala et al.[41] do not report an increase but only a drop of PL intensity of oxygen impurities with temperature, starting from ≈40 K. A drop of luminescence intensity is expected when $k_B T \approx E_A$, where E_A is the energy for thermal activation of excitons trapped at the impurity toward the free exciton state.[42] The intensity of luminescence is then described by

$$I(T) = I_0/(1 + \zeta e^{-\frac{E_A}{k_B T}}) \tag{11}$$

where I_0 is the intensity at low temperature and ζ is the ratio between thermal escape and radiative decay rates. $E_A \approx 0.033$ eV is determined in ref. [41] for O^{++}.

The intensity of PL in region C indeed shows a strong decrease. The broad emission band disappears already at ≈10 K. Such a strong drop of emission lines in the spectral region C is also reported by Jang et al.[38] Figure 7b shows another measurement at low temperatures with a smaller increment of 1 K resolving the strong drop between 7 and 10 K. At higher temperatures, a constant background remains, which may stem from a different origin. The intensity of this emission band is approximated by an exponential curve decaying from 1.95 eV to lower energies (see ref. [22]). The integrated intensity is shown in Figure 7d. A fit according to Equation (11) up to 10 K reveals an activation energy of $E_A \approx 7$ meV and $\zeta \approx 4800$. We assume that the disappearance of luminescence in region C between 10 and 12 K is related to the observed linewidth broadening and drop in oscillator strength up to 10 K (Section 3.3) as well as the increase of impurity density in Figure 6.

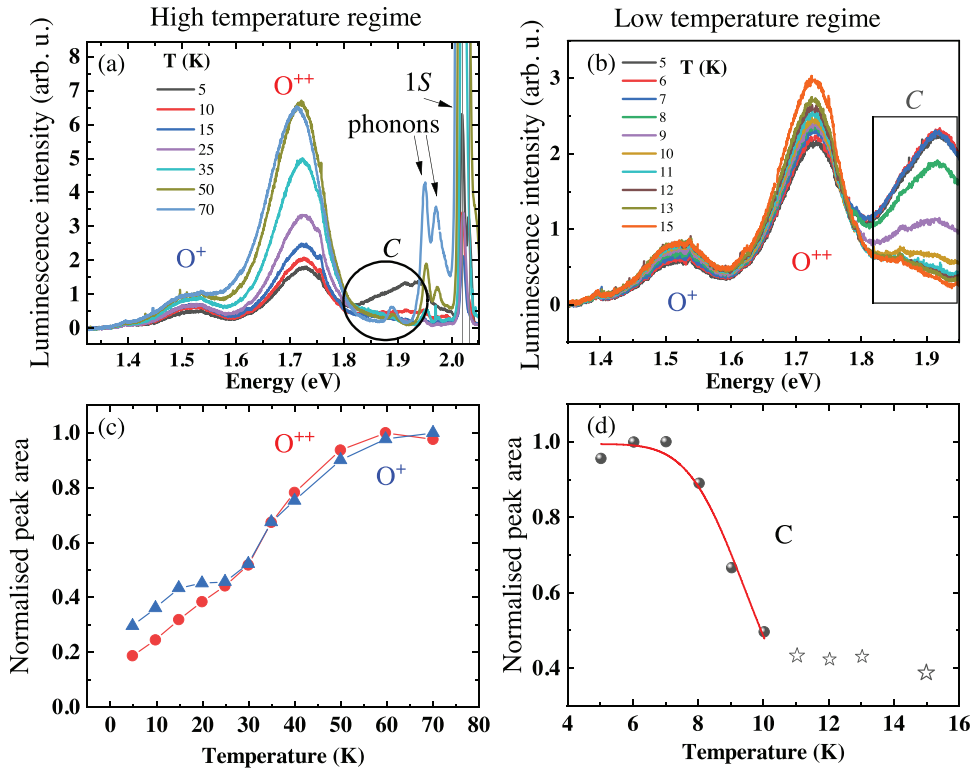

Figure 7. a) Photoluminescence spectra of oxygen vacancies (O^+, O^{++}), 1*S* exciton and Γ_3^- phonon as a function of temperature. The intensity of oxygen vacancies increases with temperature. b) Focus on impurity emission from panel (a) for low temperatures up to 15 K. A strong drop of the emission in area *C* with temperature is observed. c) Normalized spectrally integrated intensity of the O^+ and O^{++} lines in panel (a) vs temperature. d) Normalized integrated intensity of broad band emission in regions *C* as a function of temperature. The red line shows a fit according to Equation (11). Stars are excluded from fit.

4. Conclusion and Outlook

We measured and analyzed Rydberg exciton absorption spectra with quantum numbers $n \geq 10$ as a function of temperature. The narrow absorption lines of Rydberg excitons allowed us to determine the band gap shift as a function of temperature with μeV resolution and revealed a dominant contribution of the Γ_5^- phonon, in contrast to earlier reports. The linewidths and oscillator strengths of high-*nP* excitons show changes that deviate from a pure phonon scattering model. Up to ≈10 K the linewidths broaden and the oscillator strengths drop more strongly with temperature than predicted by pure phonon scattering. At these temperatures, these effects seem to be correlated with a shift of the apparent band gap $\tilde{E}_g$ (Section 3.4) from which we conclude an increasing density of charged impurities. Moreover, they also tie in with the disappearance of a particular impurity emission line (region *C*) in the same low temperature range below 15 K. We conclude that below 15 K, the presence of this type of impurities has a strong impact on the optical properties of the highest Rydberg exciton states. A comparison of n_{max} among samples of different quality is in line with the assumption of a dominant impact of impurities on the exciton spectrum and $\tilde{E}_g$ at low temperatures.

Our studies provide a new insight into the relevant contributions to the Rydberg exciton absorption spectrum at low temperatures based on experimental observations. Future investigations may aim for a comprehensive model to describe the linewidths and oscillator strength of Rydberg excitons as a function of temperature comprising the impact of phonon contributions and impurity density. To the best of our knowledge, a dependence of oscillator strength of Rydberg excitons on phonon scattering rates has not been developed yet. Such studies may improve the understanding of the optical properties of Rydberg excitons at different temperatures and separate the contributions of impurities and phonons.

Acknowledgements

The authors would like to thank D. Fröhlich for providing the samples and H. Stolz and D. Semkat for fruitful discussions. The authors acknowledge the financial support by the Deutsche Forschungsgemeinschaft through the project 504522424 and 316133134.

Open access funding enabled and organized by Projekt DEAL.

Conflict of Interest

The authors declare no conflict of interest.

Data Availability Statement

The data that support the findings of this study are available from the corresponding author upon reasonable request.

Keywords

laser spectroscopy, rydberg excitons, rydberg physics, semiconductor physics, temperature dependence

Received: December 1, 2023
Revised: February 27, 2024
Published online: April 21, 2024

[1] J. Heckötter, M. Freitag, M. Aßmann, D. Fröhlich, M. Bayer, P. Grünwald, S. Scheel, *Phys. Solid State* **2018**, *60*, 1618.
[2] C. Murray, T. Pohl, in *Advances In Atomic, Molecular, and Optical Physics*, vol. *65*, Academic Press, Cambridge, Massachusetts **2016**, 321.
[3] D. Tiarks, S. Schmidt-Eberle, T. Stolz, G. Rempe, S. Dürr, *Nat. Phys.* **2019**, *15*, 124.
[4] M. D. Lukin, M. Fleischhauer, R. Cote, L. M. Duan, D. Jaksch, J. I. Cirac, P. Zoller, *Phys. Rev. Lett.* **2001**, *87*, 037901.
[5] M. Saffman, T. G. Walker, K. Mølmer, *Rev. Mod. Phys.* **2010**, *82*, 2313.
[6] L. A. Downes, A. R. MacKellar, D. J. Whiting, C. Bourgenot, C. S. Adams, K. J. Weatherill, *Phys. Rev. X* **2020**, *10*, 011027.
[7] M. Aßmann, M. Bayer, *Adv. Quantum Technol.* **2020**, 1900134.
[8] T. Kazimierczuk, D. Fröhlich, S. Scheel, H. Stolz, M. Bayer, *Nature* **2014**, *514*, 343.
[9] M. A. M. Versteegh, S. Steinhauer, J. Bajo, T. Lettner, A. Soro, A. Romanova, S. Gyger, L. Schweickert, A. Mysyrowicz, V. Zwiller, *Phys. Rev. B* **2021**, *104*, 245206.
[10] K. Orfanakis, S. K. Rajendran, V. Walther, T. Volz, T. Pohl, H. Ohadi, *Nat. Mater.* **2022**, *21*, 767.
[11] J. Heckötter, V. Walther, S. Scheel, M. Bayer, T. Pohl, M. Aßmann, *Nat. Commun.* **2021**, *12*, 3556.
[12] C. Morin, J. Tignon, J. Mangeney, S. Dhillon, G. Czajkowski, K. Karpiński, S. Zielińska-Raczyńska, D. Ziemkiewicz, T. Boulier, *Phys. Rev. Lett.* **2022**, *129*, 137401.
[13] J. Heckötter, M. Freitag, D. Fröhlich, M. Aßmann, M. Bayer, M. A. Semina, M. M. Glazov, *Phys. Rev. B* **2017**, *96*, 125142.
[14] S. O. Krüger, H. Stolz, S. Scheel, *Phys. Rev. B* **2020**, *101*, 235204.
[15] J. Heckötter, M. Freitag, D. Fröhlich, M. Aßmann, M. Bayer, P. Grünwald, F. Schöne, D. Semkat, H. Stolz, S. Scheel, *Phys. Rev. Lett.* **2018**, *121*, 097401.
[16] D. D. Kang, A. Gross, H. Yang, Y. Morita, K. S. Choi, K. Yoshioka, N. Y. Kim, *Phys. Rev. B* **2021**, *103*, 205203.
[17] J. Heckötter, D. Janas, R. Schwartz, M. Aßmann, M. Bayer, *Phys. Rev. B* **2020**, *101*, 235207.
[18] H. Stolz, F. Schöne, D. Semkat, *New J. Phys.* **2018**, *20*, 023019.
[19] H. Stolz, D. Semkat, R. Schwartz, J. Heckötter, M. Aßmann, W.-D. Kraeft, H. Fehske, M. Bayer, *Phys. Rev. B* **2022**, *105*, 075204.
[20] P. D. Bloch, B. Meyer, C. Schwab, *J. Phys. C: Solid State Phys.* **1980**, *13*, 267.
[21] J. L. Loison, M. Robino, C. Schwab, *J. Cryst. Growth* **1980**, *50*, 816.
[22] J. Heckötter, B. Panda, K. Brägelmann, M. Harati, M. Aßmann, *Phys. Rev. B* **2023**, *108*, 235212.
[23] Y. Toyozawa, *J. Phys. Chem. Solids* **1964**, *25*, 59.
[24] T. Itoh, S.-i. Narita, *J. Phys. Soc. Jpn.* **1975**, *39*, 140.
[25] K. P. O'Donnell, X. Chen, *Appl. Phys. Lett.* **1991**, *58*, 2924.
[26] M. Grundmann, *Phys. Semicond.: An Intro. Includ. Dev. Nanophys.*, Springer, Berlin, New York **2006**.
[27] Y. Sun, G. K. L. Wong, J. B. Ketterson, *J. Lumin.* **2004**, *110*, 125.
[28] R. Pässler, *Phys. Rev. B* **2002**, *66*, 085201.
[29] Y. P. Varshni, *Physica* **1967**, *34*, 149.
[30] M. Cardona, R. K. Kremer, *Thin Solid Films* **2014**, *571*, 680.
[31] M. Giar, M. Heinemann, C. Heiliger, *Phys. Rev. B* **2017**, *96*, 075202.
[32] S. Rudin, T. L. Reinecke, B. Segall, *Phys. Rev. B* **1990**, *42*, 11218.
[33] M. Takahata, N. Naka, *Phys. Rev. B* **2018**, *98*, 195205.
[34] D. Semkat, H. Fehske, H. Stolz, *Phys. Rev. B* **2019**, *100*, 155204.
[35] D. Semkat, H. Stolz, Private Communication.
[36] T. Ito, T. Masumi, *J. Phys. Soc. Jpn.* **1997**, *66*, 2185.
[37] S. A. Lynch, C. Hodges, S. Mandal, W. Langbein, R. P. Singh, L. A. P. Gallagher, J. D. Pritchett, D. Pizzey, J. P. Rogers, C. S. Adams, M. P. A. Jones, *Phys. Rev. Mater.* **2021**, *5*, 084602.
[38] J. I. Jang, Y. Sun, B. Watkins, J. B. Ketterson, *Phys. Rev. B* **2006**, *74*, 235204.
[39] S. Steinhauer, M. A. M. Versteegh, S. Gyger, A. W. Elshaari, B. Kunert, A. Mysyrowicz, V. Zwiller, *Commun. Mater.* **2020**, *1*, 11.
[40] S. Koirala, M. Takahata, Y. Hazama, N. Naka, K. Tanaka, *J. Lumin.* **2014**, *155*, 65.
[41] S. Koirala, N. Naka, K. Tanaka, *J. Lumin.* **2013**, *134*, 524.
[42] I. Pelant, J. Valenta, *Lumin. Spectro. Semicond.*, Oxford University Press, Oxford, New York **2012**.